# Modelling of liquid metal flow and oxide film defects in filling of aluminium alloy castings

**X Dai[1*], M Jolly[1], X Yang[2], J Campbell[3]**

[1]School of Mechanical Engineering, University of Birmingham, Edgbaston, Birmingham, B15 2TT, UK
[2]School of Science and Technology, Glyndŵr University, Wrexham LL11 2AW, UK
[3]Interdisciplinary Research Centre in Materials, University of Birmingham, Edgbaston, Birmingham, B15 2TT, UK

*Corresponding author: xiaojundai@yahoo.com

**Abstract**. The liquid metal flow behaviours in different runner system designs have important effects on the mechanical strength of aluminium alloy castings. In this paper, a new model has been developed which is a two-dimensional program using a finite difference technique and the Marker and Cell (MAC) method to simulate the flow of liquid metal during filling a mould. In the program the Eulerian method has been used for the liquid metal flow, while the Oxide Film Entrainment Tracking Algorithm (OFET) method (a Lagrangian method) has been used to simulate the movement of the oxide film on the liquid metal surface or in the liquid metal flow. Several examples have been simulated and tested and the relevant results were obtained. These results were compared with measured bending strengths. It was found that the completed program was capable of simulating effectively the filling processes of different runner systems. The simulation results are consistent with the experiment. In addition, the program is capable of providing clearer images for predicting the distribution of the oxide film defects generated during filling a mould.

## 1. Introduction

The effect of liquid metal flow and surface turbulence using different designs of filling systems on the reliability of aluminium castings, and the importance of minimizing surface turbulence during filling a mould to attain reliable mechanical properties of the castings has been demonstrated by Yang et al. [1]. Their research results have shown that the proper designed running systems could maintain the ingate velocity in the range of 0.3-0.4 m/s and the final castings acquired using such runner system could obtain a greater strength. However, the use of the traditional running systems usually attains an ingate velocity well above 0.5 m/s, the critical velocity for aluminium castings [2], and the final castings have a lower fatigue strength. The results are consistent with the study conducted by Runyoro et al [3] who indicated that good quality casting could be achieved by controlling the liquid meniscus velocity below 0.5 m/s. All these studies demonstrated that there is an important relationship between the liquid aluminium flow behaviour, oxide film defect distribution, microstructures of casting defects and mechanical properties of castings for different runner systems.

Poor design of a runner system usually results in a higher priming metal flow velocity and surface turbulence so that the surface oxide films on the liquid aluminium advancing front is readily broken-up, folded-over and entrapped in the bulk liquid metal. The entrapped oxide films are frequently accompanied by different casting defects such as shrinkage pores [4], cracks and dross [5] in solidified castings.

In Al-7Si-Mg casting alloy, the casting defects associated with the oxide films may present a different morphology such as "tangled or network" [6], "layer oxide or globular oxide" [5] and "cloud or strip clustering particles" [7]. The oxide films may originate from two main sources; the stage of the melt preparation and filling. The former usually produces so-called "old" oxide films due to their formation over long time [2]. These oxide films enter a mould with careless melt preparation when using a ladle for pouring. These "old" oxide films can be entrapped and solidified in the castings to form defects in different types. However, they can be avoided by careful melt preparation. The latter, the "young" oxide films are formed in the liquid aluminium stream as it flows via the runner system into the mould in a short time [5]. As indicated by Yang et al. [1], the "young" oxide films can be broken-up and incorporated into the liquid aluminium due to surface turbulence, finally forming defects in the castings. Because of the exposure time difference of these two types of oxide films, they will present different thickness in the filling. Thiele [8] has indicated that, the thickness of oxide film measured on the liquid aluminium is 900nm at 700°C where the melt is held for 1 hour. After 5 seconds at 700°C the measured oxide film thickness on 99.5 Al is about 24 nm. When the oxidation time was increased by a factor of ten, the oxide film thickness was doubled. Therefore, the "old" and "young" oxide films can be broadly identified by their thickness.

The objective of this study is to investigate the influence of the likely oxide film defect distribution on the final mechanical strength of castings. Although the "Old" oxide films entering the mould are clearly an important source of defects in castings, their effects are in any case suppressed in this work because only differences are being assessed. The aspect of the quality of the original melt is beyond the scope of this research. Since the pouring process, and the flow of the melt through the channels that guides it into the mould cavity, last only a few seconds, the new and thin films, 'young' oxide films generated from the filling, are the concern of this investigation. Computational Fluid Dynamics (CFD) modelling was used to investigate the liquid metal flow behaviour and oxide film defect distribution in the moulds for different ingate velocities. A new numerical algorithm (2-D) – Oxide Film Entrainment Tracking (OFET) for predicting such oxide film defect distribution during the filling has been proposed. Experimental verification is undertaken by the production of Al-7Si-Mg alloy castings. Weibull statistics are employed to quantify the effects on the strength and reliability of the castings produced at two different ingate velocities, which are achieved by employing two different runner system designs. X-Ray and SEM methods were used to observe the casting defects.

## 2. Modelling of the oxide film entrainment

### *2.1. Liquid metal flow description and free surface tracking*

The liquid metal flow during the filling is basically a transient free surface flow. Assuming the molten liquid metal flow to be incompressible, the governing equations with boundary conditions can be written as free surface evolution:

$$\frac{\partial F}{\partial t}+\frac{\partial (uF)}{\partial x}+\frac{\partial (vF)}{\partial y}=0 \qquad (1)$$

where $F$ is the fractional volume-of-fluid contained in a computational cell, $u$ and $v$ are the fluid velocity components respectively. This equation states that $F$ moves with the liquid metal. Equation (1) has been employed in this investigation coupled with an oxide film entrainment tracking algorithm. When equation (1) is integrated over a computational cell, the change in F in a cell reduces to fluxes

of $F$ across the cell surfaces. The computation of fluxes is described in VOF method [9], which uses a type of donor-acceptor flux approximation to avoid the smearing of the $F$ function. The mass and momentum conservation in two-dimensional Cartesian coordinates can be expressed as:

$$\frac{\partial u}{\partial x}+\frac{\partial v}{\partial y}=0 \tag{2}$$

$$\frac{\partial u}{\partial t}+\frac{\partial (u^2)}{\partial x}+\frac{\partial (uv)}{\partial y}=-\frac{\partial p}{\partial x}+v\left(\frac{\partial^2 u}{\partial x^2}+\frac{\partial^2 u}{\partial y^2}\right)+g_x \tag{3}$$

$$\frac{\partial v}{\partial t}+\frac{\partial (uv)}{\partial x}+\frac{\partial (v^2)}{\partial y}=-\frac{\partial p}{\partial y}+v\left(\frac{\partial^2 v}{\partial x^2}+\frac{\partial^2 v}{\partial y^2}\right)+g_y \tag{4}$$

where $p$ is the ratio of pressure to the density of the liquid metal, $v$ is the kinematic viscosity, and ( $g_x$ and $g_y$ ) are body accelerations in both x and y directions, respectively. The pressure terms can be included by the use of the Poisson equation, which combines the continuity and momentum equations and reads:

$$\frac{\partial^2 p}{\partial x^2}+\frac{\partial^2 p}{\partial y^2}=-\frac{\partial D}{\partial t}-\frac{\partial^2 \left(u^2\right)}{\partial x^2}-2\frac{\partial^2 (uv)}{\partial x \partial y}-\frac{\partial^2 (v^2)}{\partial y^2}+\frac{1}{R_e}\left(\frac{\partial^2 u}{\partial x^2}+\frac{\partial^2 u}{\partial y^2}\right) \tag{5}$$

where $D$ is the velocity divergence given by the left-hand side of equation (2). The reason for incorporating the Poisson equation for pressure is that there is the lack of a direct link for pressure between continuity and momentum equations. The body accelerations are neglected in equation (5) because they are not critical to the solution of the pressure Poisson equation.

The above transport equations are discretised using the finite difference method. The transient terms are discretised using forward differencing, the convective terms are discretised using the first order upwind differencing while the pressure and diffusive terms are discretised using central differencing. The resulting linerised equations are solved using the Marker and Cell (MAC) method [10].

*2.2. Oxide film model on free surface*

A kinematic approach has been utilised for modelling the movement and entrainment of the oxide films on the liquid metal surface. Because the oxide films on the free surface are usually very thin, the inertial forces of the films can be disregarded in comparison to other forces like gravity and pressure. The Lagrangian equation describing the movement of oxide films can be written as:

$$\frac{d\vec{s}}{dt}=\vec{V} \tag{6}$$

where $\vec{s}$ and $\vec{V}$ are the displacement and velocity of a tracking point on the films, respectively. The velocities of the tracking points on the films can be determined by interpolating the velocities of the surrounding liquid metal. To ensure a proper determination of the positions of the films, sufficient tracking points are introduced. At time step n, the locations and the velocities of the tracking points can be obtained from the flow calculation. The positions of these points for next time step n+ 1 can be determined by the following equations:

$$x_i^{n+1}=MIN\{x_i^n+0.5(u_i^n+u_i^{n+1})\Delta t+CX, x_{is}^{n+1}\}$$

$$y_i^{n+1}=MIN\{y_i^n+0.5(v_i^n+v_i^{n+1})\Delta t+CY, y_{is}^{n+1}\} \tag{7}$$

and where

$$CX = MAX\{x_{is}^{n+1} - (x_i^n + 0.5(u_i^n + u_i^{n+1})\Delta t), 0.0\}$$

$$CY = MAX\{y_{is}^{n+1} - (y_i^n + 0.5(v_i^n + v_i^{n+1})\Delta t), 0.0\} \quad (8)$$

where $x_{is}^{n+1}$ and $y_{is}^{n+1}$ are the points which represent the liquid metal free surface as shown in Figure 1. The MIN feature in Eq. (7) prevents the displacement of the films out of the advancing free surface while the MAX feature readjusts those points back to the surface. In Figure 1, the points with the symbol "⊗" which are joined by the dashed curve represent the positions of tracking points at time step n+1 without utilising the MIN and MAX features. The solid curves with the symbols "①" and "②" indicate the liquid metal free surfaces obtained by the VOF method at time steps n and n+1.

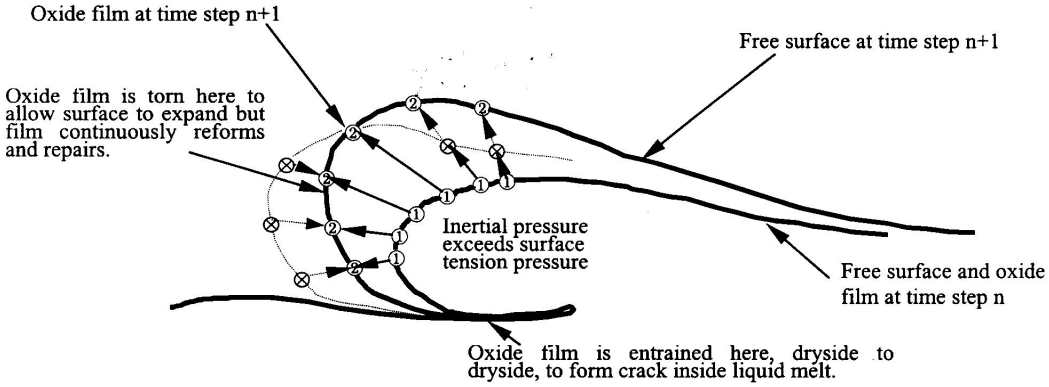


**Figure 1.** Tracking points on the oxide film at time steps n and n+1, the oxide film points are located at the end of arrows.

The surface segments, which consist of the tracking points, are considered as film elements. In the simulation, a surface normal that is pointing away from the dryside of the surface element is introduced. If the local inertial pressure is larger than the restraining pressure, the oxide film will be torn but the film continuously reforms and repairs to allow the free surface to expand. A new tracking point is then added to account for the newly formed oxide film which bridges the surrounding track points. After new tracking points are added, all tracking points are renumbered. If the surface normal for the oxide film elements is pointing against each other, the oxide films, dry side to dry side, are considered to be entrained into the flow [2]. In doing so, all the tracking points for the film elements have to be renumbered consecutively and a numerical algorithm to judge such fold over is proposed accordingly as described in Section 2.3.

For the movement of films already entrapped in the liquid metal, the following equation is used.

$$x_i^{n+1} = x_i^n + 0.5(u_i^n + u_i^{n+1})\Delta t$$
$$y_i^{n+1} = y_i^n + 0.5(v_i^n + v_i^{n+1})\Delta t \quad (9)$$

The treatment of films entrapped in the melt will be slightly different from treating those films on the free surface. It is assumed that once the oxide films are torn, there is no need to introduce new tracking points since no oxygen is available for the creation of more oxidised surface. This assumption neglects the real contribution that might be made by the air entrained between the double film, either trapped in macroscopic enclosed folds or bubbles, or as contained in the microscopic roughness of the oxide crystals.

*2.3. Oxide film entrainment and fold over judgement - the numerical algorithm (OFET)*

As shown in Figure 1, when the reflected liquid from the walls of the mould forms a backward rolling wave overlying the underneath stream, the oxide films are folded into the liquid metal, dry side to dry side. A careful observation of this phenomenon reveals that the velocities for these two overlaid opposite flowing streams are always opposite. This information can be used to judge whether or not the oxide films are entrained and folded. Suppose that the fold over has taken place as shown in Figure 2. The velocities at both the top and bottom of the computational cell are employed.

$$F_{oxide} = \mathrm{sgn}\left[ \min\left( \frac{u_{i+\frac{1}{2},j+1}}{u_{i+\frac{1}{2},j}}, \frac{v_{i+\frac{1}{2},j+1}}{v_{i+\frac{1}{2},j}} \right) \right] \tag{10}$$

where $u_{i+\frac{1}{2},j}$ and $u_{i+\frac{1}{2},j+1}$ are the x-direction velocity components, and $v_{i+\frac{1}{2},j+1}$ and $v_{i+\frac{1}{2},j}$ are the y-direction velocity components at the bottom and top sides of the cell. The sgn function determines the sign of the smaller ratio between the velocity components. If $F_{oxide}$ is negative, an oxide film entrainment or fold over is judged to occur. If $F_{oxide}$ is positive, no oxide film fold over happens. The above OFET algorithm is expected to predict qualitatively the distribution of oxide films in the casting.

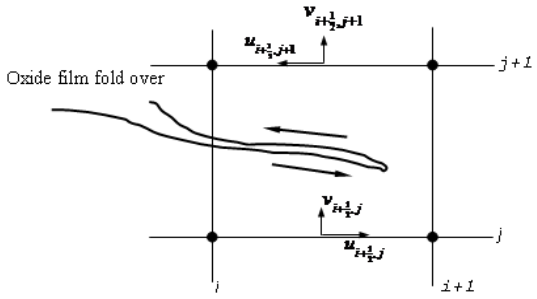


**Figure 2.** A sketch of how to judge the oxide film fold over

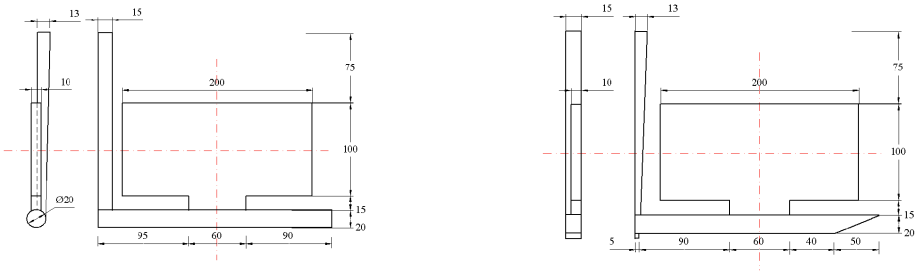


(a) (b)

**Figure 3.**Runner systems (a) Vortex-flow runner system(b)Rectangular runner system

## 3. Experimental investigation

*3.1. Runner system design*

Two different runner system designs with dimensions: Vortex-flow Runner (VR) and Rectangular Runner (RR) are shown in Figure 3. Each runner system includes a pouring basin, a tapered sprue, a runner, a gate and a mould cavity. It can be seen that the only difference between the runner systems is the cross-sectional shapes of the runners. This arrangement allows a direct comparison of the liquid metal flow behaviour and the performance of the castings made using different runner systems.

*3.2. Casting aluminium alloy and module materials*

Commercial aluminium alloy (Al-7Si-0.4Mg) was used to make the castings. Four castings were poured, two for each runner system. All the castings were poured at a temperature of 735-740˚C. After casting, all the samples were subjected to heat at 540˚C for 6 hours and quench in hot water (80-90˚C), then precipitation hardened at 160˚C for 6 hours. Chemically bonded silica sand with AFS fineness 60 and PEPSET process was used to make the mould.

*3.3. Mechanical strength test*

All the castings were machined into four-point bend specimens as shown in Figure 4. The Four-point Bend Test method was employed as shown in Figure 5.

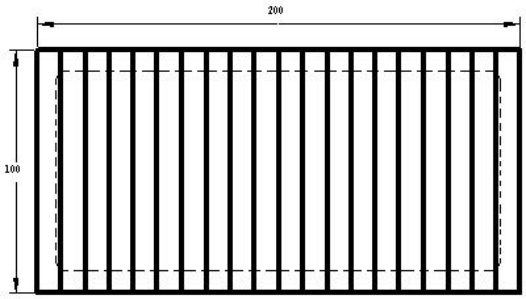


**Figure 4.** The sampling plan for cast plates, producing specimens for Four-Point Bend Test

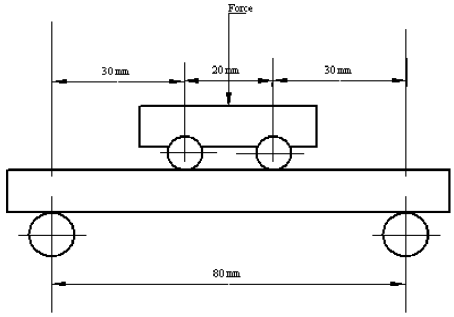


**Figure 5.** The sketch of Four-Point Test adopted in this work.

*3.4. Observation of X-ray and SEM observation*

The macroscopic defect distribution in the castings for both VR and RR runner systems was viewed by X-ray radiography. The SEM method was used to observe the micro defects on the polished fracture surface of specimen from RR runner casting

## 4. Results

Based on the previous work [1], the maximum flow velocity in the ingate is at the right-hand edge for both the VR and RR runner at the moment when the liquid metal front enters the mould, with the value reaching 0.4 m/s and 0.7 m/s in the cases of VR and RR runners, respectively. In the case of VR runner system, the metal velocity was maintained below 0.5 m/s for the entire filling time.

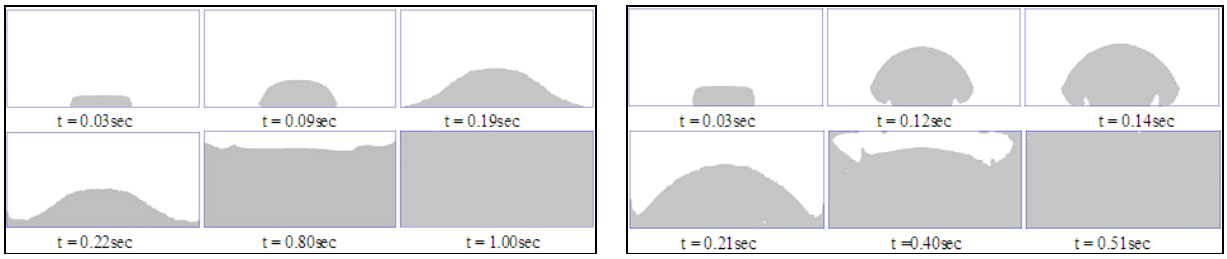


(a) (b)

**Figure 6**. Numerical simulations of filling processes for the two different filling systems; (a) VR runner system; (b) RR runner system.

Numerical simulations of the filling processes for the case of two different filling geometries are shown in Figure 6a, 6b. It can be seen from Figure 6a that the liquid metal flow for the ingate velocity 0.4 m/s (equivalent to the use VR runner system) is smooth, and neither splash nor folding-over of the melt can be observed when the liquid aluminium enters the mould cavities. In contrast to the case of 0.4 m/s, the liquid metal flow in the case of ingate velocity 0.7 m/s, using RR runner system,

(Figure 6b) exhibits an undesirable behaviour: the melt fountains and folds over, thus giving rise to the possibility of generating surface turbulence, which might potentially entrap oxide film defects.

Corresponding to Figure 6, the predicted distributions of entrapped oxide films in the castings using the OFET numerical algorithm are shown in Figure 7a and 7b. It can be seen from Figure 7a that the predicted susceptible oxide film defects are basically excluded from the internal zone of casting, and most of the oxide films are distributed around the edge of the casting. This implies a better mechanical strength of the castings since the bend test assesses the central areas. Figure 7b clearly shows that the entrained oxide films are concentrated into the body of the castings. The frequency plots of the UBS for specimens from Figure 4 are shown separately in Figure 8a and 8b. Figure 8c shows the corresponding Weibull plots. The lower values in the two plots represent the specimens taken from the central area of the castings. Specimens taken from the edge area of castings show higher strength values due to the "edge effect".

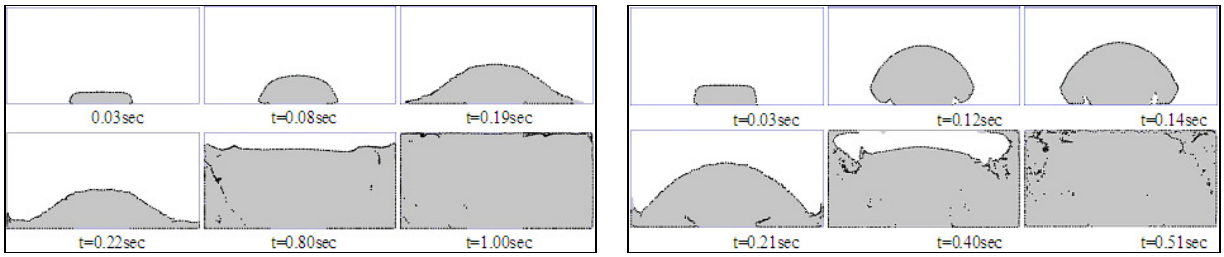


(a) (b)

**Figure 7.** Predicted susceptible oxide film defect distribution in the castings by using the OFET numerical algorithm. (a) VR runner system; (b) RR runner system.

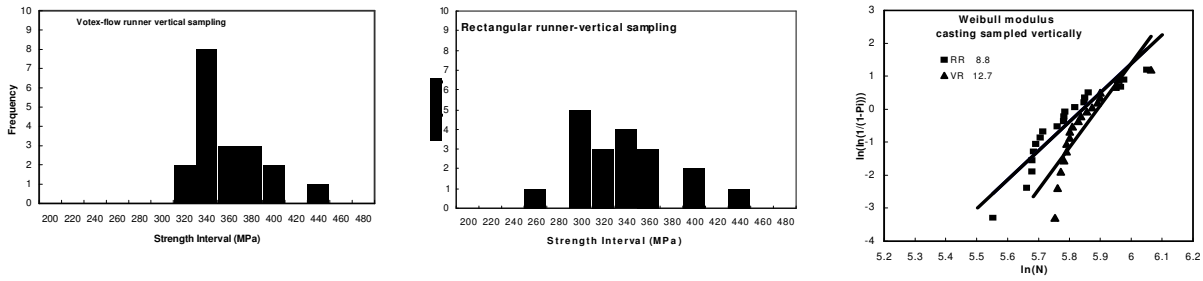


(a) (b) (c)

**Figure 8**. (a)UBS distributions of VR runner system; (b) UBS distributions of RR runner system; (c) Weibull plots of all the casting specimens UBS.

For vertical sampling, the Weibull moduli (the slope of the line) of the respective sets of specimens are 12.7 and 8.8. The Weibull moduli shown in Figure 8c indicate the average strength and the reliability of the castings for VR filling system is higher than that of the RR system.

Figure 9 shows the distribution of defects in the casting samples obtained using RR runner system. The shrinkage porosity distributions concentrate in the area closed to the ingate of the casting sample in the RR runner system. The radiographic image of the VR plates were featureless and are consequently not shown.

In Figure 10 SEM micrographs show the distribution of defects on the polished fracture surface of specimen from RR runner casting where Figure 10a show a tangled network of oxide films and Figure 10b is a close view of Figure 10a with gas between the double layer type oxide film.

Figure 11 shows the oxide films on the fracture surface of RR specimen using SEM method.

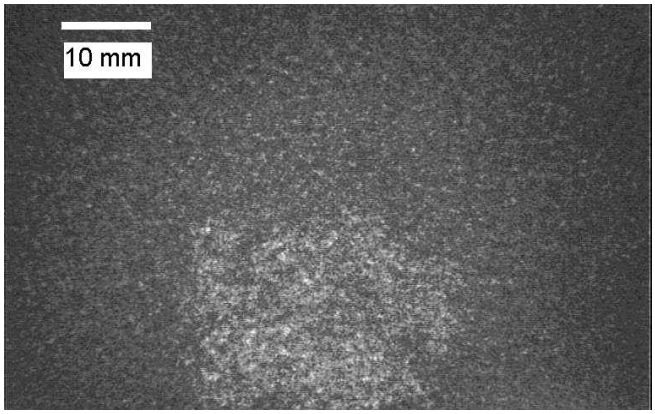


**Figure 9.** X-ray Radiographic showing the distribution of shrinkage porosity in the castings where is close to the ingate of cast plate (RR).

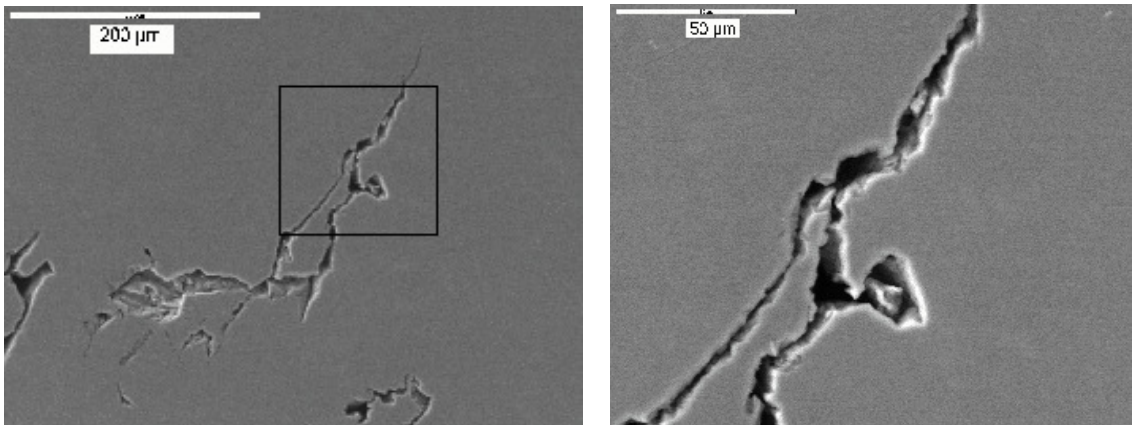


(a) (b)

**Figure 10.** SEM micrographs show the distribution of defects on the polished fracture surface of specimen from RR runner casting; (a) show a tangled network of oxide films; (b) is a close view of (a) with gas between the double layer type oxide film.

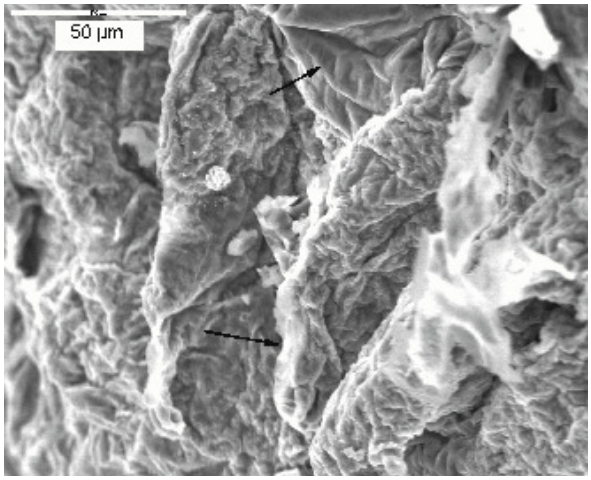


**Figure 11.** The oxide films shown on the fracture surface of a RR specimen using SEM method

## 5. Discussion

Based on the OFET simulations, the oxide film defects are occurring around the outer surface of the casting for the VR case while they are entrained into the central part of the casting for the RR case. However, the entrainment of the oxide films into the casting for the case of ingate velocity of 0.7 m/s are expected to influence the final mechanical strength of those samples in the central part of the casting.

The results for the case of ingate velocity of 0.7 m/s (the RR running system) are consistently poorer when judged by oxide film entrainment tracking simulation, strength, Weibull modulus, or by microstructure observed by using X-ray radiograph and SEM methods. This consistency strongly suggests that the castings filled with a higher ingate velocity, in particular greater than the critical velocity of 0.5 m/s, are most likely defective. Indeed, it was observed from the simulations that when the ingate velocity is greater than 0.5 m/s, the melt certainly forms fountain and folds over, thus generating the surface turbulence. This could be especially important in the brief but vulnerable period especially when the runner is still priming and the melt is just entering the mould through the ingate, so that there is freedom for the melt to jump and splash, creating additional area for the creation of new films.

The outstandingly robust result of the use of lower ingate velocity (the VR running system) demonstrated again that once the ingate velocity is less than the critical velocity of 0.5 m/s, the liquid metal fountaining, which may contribute to the generation of surface turbulence, could be avoided. This is the condition of the Weber number being smaller than unity. In order to convert the high velocity of the liquid metal at the exit of the sprue into a relatively gentle and smooth stream, advancing with a velocity less than the critical velocity for the entrainment of the surface as the metal enters the mould cavity, the filling system has to be effective in dissipating sufficient kinetic energy of the liquid metal. The use of vortex flow runner (VR) can generate a strong ordered movement of the liquid as it enters the runner via the sprue. The ordered behaviour extends along the length of the runner, assisting the reduction of ingate velocity as a result of the considerable dissipation of energy by the rapid rotation.

The above results demonstrate the vital role played by oxide films during the filling of the mould. The results confirm the expectations as indicated in the introduction, that the "young" oxide films are closely related to surface turbulence. Thus, a reduction in surface turbulence will reduce the possibilities of free surface break-up and the entrapment of surface oxide films. It seems that by optimising the runner system design and improving the flow behaviour during the filling, the fluid velocity in the ingate can be reduced to be less than the critical velocity 0.5m/s and the entrainment of "young" oxide films into the castings can be significantly reduced so that the mechanical strength and reliability of aluminium alloy castings can be enhanced.

## 6. Conclusions

A numerical algorithm – Oxide Film Entrainment Tracking (OFET, 2-D) for forecastingthe oxide film defects distribution in the liquid aluminium throughout the filling is proposed and incorporated into the free surface tracking code developed for simulating filling. It is found from numerical simulation that the number and distribution of the oxide film defects generated from filling are significantly affected by ingate velocities. The reduction of ingate velocity can effectively reduce casting defects, while this can be achieved by controlling the disordered behaviour of liquid metal flow and by dissipating the kinetic energy of the metal in the runner. The simulation results were validated using the methods of bending strength test and micro casting defect observation.

**Acknowledgements**
The authors wish to acknowledge the support of the EPSRC under contract GR14507/01. Many thanks to the assistance of Mr David Cloney, Mr John Turner, Mr Willie Logan and Ms Margaret Corrigan for assisting in the preparation of the mechanical strength test and SEM images.

**References**

[1] Yang X, Jolly M and Campbell J 2000 Minimisation of surface turbulence during filling using a vortex-flow runner *Aluminium Trans* **2** 61-80
[2] Campbell J 1991 *Casting*, (Oxford: Butterworth-Heinemann)
[3] Runyoro J, Boutarabi S M and Campbell J 1992 Critical Gate Velocities For Film Forming Casting Alloy: a Basis for Process Specification *AFS Trans* **102** 225-234
[4] Cáceres C H and Selling B I 1996 Casting defects and the tensile properties of an Al-Si-Mg alloy *Mat Sci Engng A* **220** 109-116
[5] Divandari M 2001 Mechanisms of bubble damage in castings *PhD Thesis* University of Birmingham 12-16
[6] Green N R and Campbell J 1994 Influence of Oxide Film Filling Defects on the Strength of Al-7Si-Mg Alloy Castings *AFS Trans* **114** 341-347
[7] Huang W L, Shu J W and Shih S T 2000 Diagnosis and Analysis of Oxide film in Al-Si-Mg Alloys *AFS Trans* **40** 547-560
[8] Thiele W G 1962 *Aluminium* **38** 707-715, 780-786 (Translation)
[9] Hirt C W and Nichols B D 1981 *J Comput Phys* **39** 201-225
[10] Harlow F H and Welch J E 1965 *Phys of Fluid* **8-12** 2182-2189

# Modelling of liquid metal flow and oxide film defects in filling of aluminium alloy castings

Dai, Xiaojun J.

2012-12-31T00:00:00Z

X Dai, M Jolly, X Yang, J Campbell. IOP Conference Series: Materials Science and Engineering, Volume 33, Conference 1, 2012, Paper Number: 012073
http://dx.doi.org/10.1088/1757-899X/33/1/012073